# Low-Earth Orbit User Segment in the Ku and Ka-Band

## An Overview of Antennas and RF Front-End Technologies

Amendola, Giandomenico; Cavallo, Daniele; Chaloun, Tobias; Defrance, Nicolas; Goussetis, George; Margalef-Rovira, Marc; Martini, Enrica; Quevedo-Teruel, Oscar; Valenta, Vaclav; More Authors

**DOI**
10.1109/MMM.2022.3217961

**Publication date**
2023

**Document Version**
Final published version

**Published in**
IEEE Microwave Magazine

# Low-Earth Orbit User Segment in the Ku and Ka-Band

*Giandomenico Amendola, Daniele Cavallo, Tobias Chaloun, Nicolas Defrance, George Goussetis, Marc Margalef-Rovira, Enrica Martini, Oscar Quevedo-Teruel, Václav Valenta, Nelson J.G. Fonseca, and Mauro Ettorre*

Low-Earth orbit (LEO) constellations are revolutionizing the world of satellite communication (Satcom), providing new opportunities to manufacturers and operators and enabling innovative and attractive services to users. The main advantages of low-orbit satellite systems are

- more extended coverage of the surface of Earth that permits the availability of Satcom links in areas not served by geostationary Earth orbit (GEO) systems
- reduced latency that proves to be fundamental for real-time and mission-critical applications

*Giandomenico Amendola (g.amendola@dimes.unical.it) is with the Dipartimento di Ingegneria Informatica, Modellistica, Elettronica, e Sistemistica, Università della Calabria, 87036 Rende (CS), Italy. Daniele Cavallo (d.cavallo@tudelft.nl) is with the Department of Microelectronics, Faculty of Electrical Engineering, Mathematics, and Computer Science, Delft University of Technology, 2628 CD Delft, The Netherlands. Tobias Chaloun (tobias.chaloun@uni-ulm.de) is with the Institute of Microwave Engineering, Ulm University, 89081 Ulm, Germany. Nicolas Defrance (nicolas.defrance@univ-lille.fr) is with Université de Lille, CNRS, Centrale Lille, Université de Polytechnique Hauts-de-France, IEMN–Institut d'Électronique de Microélectronique et de Nanotechnologie, F-59000 Lille, France. George Goussetis (g.goussetis@hw.ac.uk) is with the School of Engineering and Physical Sciences, Institute of Sensors Signals and Systems, Heriot–Watt University, Edinburgh EH14 4AS, U.K. Marc Margalef-Rovira (marc.margalefrovira@univ-lille.fr) is with Université de Lille, CNRS, Centrale Lille, Université de Polytechnique Hauts-de-France, IEMN–Institut d'Électronique de Microélectronique et de Nanotechnologie, F-59000 Lille, France. Enrica Martini (martini@dii.unisi.it) is with the Department of Information Engineering and Mathematics, University of Siena, 53100 Siena, Italy. Oscar Quevedo-Teruel (oscarqt@kth.se) is with the Division of Electromagnetic Engineering, KTH Royal Institute of Technology, 11428 Stockholm, Sweden. Vaclav Valenta (vaclav.valenta@esa.int) is with European Space Research and Technology Center, European Space Agency, 2201 AZ, Noordwijk, The Netherlands. Nelson J.G. Fonseca (nelson.fonseca@esa.int) is with the Antenna and Sub-Millimeter Waves Section, European Space Agency, 2200 AG Noordwijk, The Netherlands. Mauro Ettorre (mauro.ettorre@univ-rennes1.fr) is with Université de Rennes, CNRS, IETR, 35000 Rennes, France.*

*Digital Object Identifier 10.1109/MMM.2022.3217961*
*Date of current version: 5 January 2023*

©SHUTTERSTOCK.COM/NICOEININO

- reduced size of user terminals, due to the reduced path loss of low-orbit satellites.

However, the benefits given by LEO satellites come with technical challenges. LEO satellites travel at high speed and can ensure the coverage of targeted areas of Earth's surface only for a limited time, placing stringent requirements on the antenna for both the space and ground segments. In particular, the antennas should be agile and able to steer their main beam over a large field of view. This field of view of the antenna is related to the number of satellites in the constellations. A tradeoff is therefore required to achieve a reasonable number of satellites and a feasible field of view for robust communications. Furthermore, LEO systems require handovers among satellites to guarantee uninterrupted links, at the cost of a more complex system. The handovers are achieved by radiating several beams and by buffering the information in the antenna terminal.

LEO links alleviate some of the drawbacks of GEO systems but give new technological challenges in the design of antenna systems and RF front ends. The present article attempts to provide a broad overview of the available RF technologies that allow designers to tackle these challenges and help build the future LEO user segment. The article develops in six sections. The "Ku and Ka LEO Systems" section presents a brief account of the current LEO systems at the Ku-/Ka-band by reviewing present and future constellations and providing information relevant to the development of the user segments. The "Characteristics of LEO Terminals" section defines very general requirements corresponding to a Starlink-like LEO system. Also, in this section, we identify the technologies presented in the following parts of the review. In a nutshell, the article follows the structure of an RF front end, starting from the antenna and going down toward the other components. For brevity, we have reduced the scope of this review to antennas, beamforming technologies, low-noise amplifiers (LNAs), and power amplifiers (PAs). Notice that there are fields of research that are equally important and not included in the present work. As an example, the areas of packaging and integration, which is of utmost

importance to provide highly integrated solutions, and analog phase shifters will not be treated in this article.

In the "Antennas" section, we review the most recent antenna solutions suited to LEO communications. We present the antennas according to the scanning approach: mechanical and fully electronic. In the "Beamformers" section, we discuss state-of-the-art beamforming technologies. We include analog passive beamformers and silicon (Si) active beamformers, as they are becoming a fundamental building block of electronically steerable antennas. As a final contribution, we account for recent developments in digital beamforming (DBF). While DBF is not identifiable with one single device, it is one of the most promising technologies related to phased arrays and multibeam antennas for future LEO space and ground segments. Finally, the "Semiconductor Technologies" section reports the most relevant performance of LNAs and PAs.

## Ku and Ka LEO Systems

Despite the large investments dedicated to the development of LEO constellations, technical information about the communication technology adopted on board satellites is rather scarce. In this section, we summarize data available in the open literature to constitute a framework into which all the information reported in the following paragraphs can be placed. We consider constellations that are already in operation and in advanced development stages, for example, Starlink, OneWeb, Telesat, and Kuiper [1], [2], [3]. The main constellation parameters are reported in Table 1. The four constellations will be deployed in LEO, with altitudes that may change according to the orbital planes to which the satellites are allocated. Both user and feeder links operate in Ku and/or Ka frequency bands allocated to Satcom communications. Table 1 reports information that can be used in a simplified link budget estimation. The data reported in Table 1 indicate that the onboard resources provided by the constellations are abundant and, in most cases, thanks to the multispot approach and the reduced altitude of the orbits, the design of compact and effective user terminals is possible.

## Characteristics of LEO Terminals

The specifications of Satcom terminals vary greatly depending on the application and the data rate. The following section describes some of the characteristics of terminals with bit rates higher than 20 Mb/s, which are typical of broadband Internet access services. Table 2 shows indicative Ku-band link budgets for the downlink and the uplink that consider a download data rate of 100 Mb/s and upload rate of 20 Mb/s [4]. The satellite parameters are the ones of the Starlink constellation reported in [1] and [2], which used U.S. Federal Communications Commission filings as sources. The diameter of the antenna is 0.7 m, with the aperture efficiency set to 30% to include the case of planar phased-array antennas. The receive (Rx) RF front end has a 1-dB interconnection loss and a 3-dB noise figure (NF). The downlink budget reported in Table 2 shows that the link margin at 99.9% availability is more than 6 dB. Note that even considering a receiver with a 6-dB NF and including a scanning loss of 3 dB, the calculated link margin is greater than 2 dB.

**TABLE 1. The main parameters of the Telesat, OneWeb, Starlink, and Kuiper constellations [1], [2].**

| | Telesat | OneWeb | Starlink | Kuiper |
|---|---|---|---|---|
| Number of satellites (first phase full constellation) | 298 (1,671) | 716 (6,372) | 1,584 (4,408) | 578 (3,236) |
| Altitude | 1,015–1,325 km | 1,200 km | 550–570 km | 590–630 km |
| User link frequencies | Up: 27.5–30 GHz<br>Down: 17.8–20.1 GHz | Up: 12.75–14.5 GHz<br>Down: 10.7–12.7 GHz | Up: 14–14.5 GHz<br>Down: 10.7–12.7 GHz | Up: 28.35–30 GHz<br>Down: 17.7–20.1 GHz |
| | | Downlink | | |
| | Telesat | OneWeb | Starlink | Kuiper |
| Number of user beams | ≥16 | 16 | ≥16 | ≥16 |
| Channel bandwidth | <400 MHz | 250 MHz | 250 MHz | 100 MHz |
| Maximum antenna gain | 38 dB | N/A | 37.1 dB | 39 dB |
| Maximum EIRP | 39 dBW | 34.6 dBW | 32.71 dBW | 43.1 dBW |
| | | Uplink | | |
| | Telesat | OneWeb | Starlink | Kuiper |
| Channel bandwidth | <400 MHz | 125 MHz | 125 MHz | 50 MHz |
| Maximum antenna gain | 37.1 dB | N/A | 37.1 dB | 39 dB |
| Maximum G/T | 13.2 dB/K | –1 dB/K | 9.8 dB/K | — |

EIRP: effective isotropic radiated power; dBW: decibel watt; G/T: antenna gain-to-noise-temperature.

The uplink budget considers a circular aperture with a diameter of 0.35 m and 5 W of RF input power. This configuration roughly corresponds to a circular array of about 900 elements spaced at half a wavelength, fed with one amplifier per element, with 7.5 dB referenced to 1 mW (dBm) of output power at a 1-dB compression point. The antenna aperture efficiency is 25%, lower than the one used in the Rx case to account for the higher frequency of the transmit (Tx) band. Table 2 shows that the link margin is more than 6.4 dB and leaves room for a 3-dB scan loss.

The evaluations presented in the preceding confirm that link budgets may be closed, considering components with performance that is compatible with the state of the art. However, considerable R&D efforts are still needed to design compact and flexible terminals. The difficulties mainly come from the requirement of scanning at low elevation angles and radiating two simultaneous beams. The difficulties dramatically increase if one must integrate Tx and Rx operations into a single aperture.

The architecture of the RF front end of a ground terminal may change according to the antenna and the beamforming techniques that may combine to adapt to diverse requirements. Even if any attempt at a classification gives a partial view of all possible combinations, we refer to the categorization shown in Figure 1. Since LEO terminals must continuously scan their beam toward moving satellites, the classification is according to the beam scanning techniques. In the subsequent

**TABLE 2. The downlink and uplink budgets for a Starlink-based terminal.**

| Downlink | | Uplink | |
|---|---|---|---|
| **Data Rate** | **100 Mb/s** | **Data Rate** | **20 Mb/s** |
| Frequency | 11.5 GHz | Frequency | 14 GHz |
| Satellite EIRP | 32.71 dBW | Satellite G/T | 9.8 dB/K |
| MODCOD | 16-APSK(3/4) | MODCOD | 16-APSK(3/4) |
| Roll off | 0.2 | Roll off | 0.2 |
| Elevation | 40° | Elevation | 40° |
| Path loss | 168.47 dB | Path loss | 170.18 dB |
| Atm. + rain loss | 1.89 dB | Atm. + rain loss | 2.97 dB |
| Rx antenna gain | 33.3 dB | Tx antenna gain | 28.19 dB |
| Rx antenna temperature | 71.73 K | Tx antenna temperature | — |
| Rx antenna G/T | 6.19 dB | Tx pin: 1 dB | 5 W |
| C/ASI | 25 dB | C/ASI | 25 dB |
| C/XPI | 22 dB | C/XPI | 22 dB |
| C/IM | 25 dB | C/IM | 25 dB |
| Eb/(N0 + I0) | 11.51 dB | Eb/(N0+I0) | 11.87 dB |
| Eb/N0 | 5.5 dB | Eb/N0 | 5.5 dB |
| Link margin: 99.9% average | 6.01 dB | Link margin: 99.9% average | 6.37 dB |

MODCOD: modulation and coding; APSK: amplitude phase shift key; Atm: atmospheric: C/ASI: carrier to adjacent satellite interference; C/XPI: carrier to cross polarization interference; C/IM: carrier to intermodulation interference; Eb/N=: energy per bit over noise ratio; Eb7N0+I0: energy per bit over noise plus interference ratio.

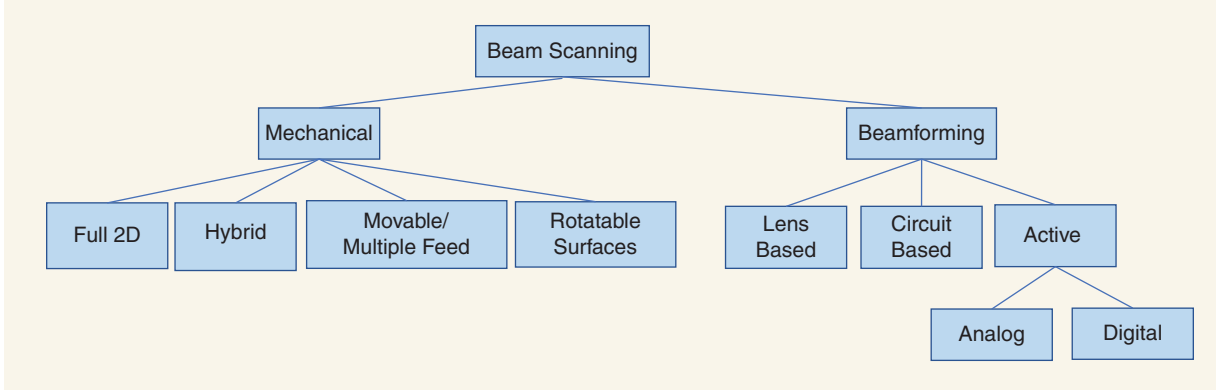


**Figure 1.** *The classification of antennas and beamforming techniques.*

sections, Figure 1 is used as a reference for reviewing antennas, beamforming, and semiconductor technologies for LEO terminals.

## Antennas

Because LEO systems require terminals able to follow satellites along their orbits, we classify antennas according to their scanning mechanism, considering two very broad categories: mechanically scanned antennas and electronically scanned antennas. These two approaches present different degrees of maturity, performance, and cost. In the following, the two categories are presented briefly, explaining their principle of operation and describing their performance.

### *Mechanical Scanning*

Mechanically scanned antennas offer extended angular coverage with excellent performance in terms of polarization purity, the band of operation, and the antenna gain-to-noise-temperature (G/T) figure. Figure 1 proposes a classification of the available technologies that groups mechanically scanned antennas into four broad classes: based on gimbals, allowing full 2D mechanical pointing, hybrid systems, moving feeds, and rotatable surfaces. The same classification is followed in the subsequent sections to present the characteristics of the antenna systems. Note that this classification is inevitably stretched, and while it covers most of the systems in use, it does not encompass all possible configurations, such as the class of hybrid systems, which covers more than one of the highlighted groups.

#### Full 2D Pointing Systems

Full 2D pointing requires complex mechanical gimbals. Many of these solutions rely on conservative concepts, such as reflector antennas [5], [6]. Such antennas are generally bulky and heavy and may require a gimbal with at least two servomotors to control the pointing direction of the radiated beam and its polarization. Over the years, the profile of mechanically steered antennas has been reduced to ease their integration in moving platforms, such as airplanes. Solutions based on waveguide-based arrays [7] have been adopted because they have a lower profile and better efficiency than reflector antennas. However, they require complex pointing mechanisms that couple azimuthal rotation with movement in elevation.

#### Hybrid Systems

The complexity of 2D pointing systems is reduced when considering hybrid systems in which only the azimuthal rotation is achieved mechanically. Pointing in elevation is obtained by scanning the beam by using conventional phase shifters, quasi-optical beamformers, and, in the case of lens antennas, adopting multifeed systems and moving feeds. The final two cases are described in the following sections.

Different designs have been proposed in recent years for the Ku-band in which a planar array is integrated with phase shifters to scan the beam in one direction, [8], [9]. In [10], elevation beam steering is obtained through a switched-beam architecture realized in microstrip technology in the form of a Rotman lens. Employing RF switches instead of phase shifters implies lower losses, higher simplicity, and lower cost. Planar quasi-optical beam formers, such as the Rotman lens, also have the advantage of being able to generate simultaneous independent beams, which can be used to realize a make-before-break handover between different satellites. Furthermore, their design generally relies on nonresonant true-time delay structures and is therefore intrinsically broadband. In particular, this implies that Tx and Rx functions can be combined into the same aperture, possibly covering multiple bands. Lens-based concepts in parallel plate waveguide (PPW) technology have been introduced in the Ka-band to preserve the wideband operation of reflector-based solutions and, at the same time, provide a wide coverage (±50° in elevation) [11]. Arrays based on a long slot fed by multimode PPWs, proposed in [12] and [13], show polarization agility, at the cost of a complex design process, a field of view of ±45° in elevation, and a reduced bandwidth (29–32 GHz)

#### Movable Feeds and Multifeed Systems

Another class of mechanically scanned antennas suitable for Satcom communications are volumetric lenses using movable feeds and multifeed systems. They are seen as quasi-optical beamformers that may achieve a wide scan range with reduced antenna dimensions compared to reflectors. Volumetric lenses can be classified into two main categories:

1) homogeneous lenses [14], whose scan range is limited by aberrations
2) graded-index lenses, which can be aberration-free.

Classical designs of graded-index lenses allowing beam scanning, such as the Luneburg lens and the half Maxwell fish eye lens [15], do not meet the low-profile requirement and may not be suitable for Satcom applications, such as Satcom on the move. Arrays of smaller lenses can offer better efficiency than a single lens of a similar aperture, with a lower profile [16]. In recent years, the application of transformation optics concepts [17] was proposed to reduce the profile of the Luneburg lens. Scanning is obtained simply by displacing the feed, at the price of an increased scanning loss and a reduction of the scanning range [18], [19].

A 2D version of the Luneburg lens can provide full azimuthal coverage with a low-profile arrangement, and it can be used as a beamforming network for a radiating aperture. Practical realizations are normally done in PPW technology. Different solutions have been proposed to realize the required effective refractive index variation. This can be achieved by machining a distribution of metal posts between PPW plates [20], photolithographically etching holes into one side of a standard printed circuit board ground plane [21], and loading the parallel plates with electrically small patches printed on a grounded dielectric slab [22]. A similar metasurface-based solution has been used in [23] to implement a half Maxwell fish eye lens. All-metal lenses realized with a bed of nails and by periodic holes in a thick metallic plate have also been presented [24], [25]. An alternative fully metallic solution is obtained in [26], relying on a geodesic approach. This solution has the advantage of increased bandwidth compared to the approaches based on dispersive modulated metasurfaces. Furthermore, it is scalable to high frequencies, due to the lack of small geometric details. However, it has a larger thickness when compared with its fully planar counterparts. Note that in all the 2D lenses reported until now, scanning is achieved by displacing the feed and by implementing a multifeed system.

### Rotatable Surfaces Systems

Low-profile antennas with full 2D scanning may be implemented using rotatable surfaces. The best-performing antenna terminals in the Ku- and Ka-bands in this category are designed by ThinKom. ThinKom's antennas are based on variable-inclination continuous transverse stub (VICTS) technology, an array of stubs rotating around a single axis for a wide field of view and operating band [27], [28]. The terminal provides interoperability among different constellations, with a large field of view (7.5–90° in elevation) and very appealing G/T performance (>12 dB/K at a 20° elevation). Mechanical solutions do not generally have multiple-beam radiation. Information is, then, buffered to switch among satellites requiring rapid control of the radiated beam.

2D scanning is also achieved with rotatable graded-index lenses placed in front of a radiating aperture. The principle of operation is similar to the so-called Risley prisms. In this solution, a fixed primary radiator with a broadside pencil beam illuminates two parallel planar lenses, providing a linear phase shift. The two lenses can be rotated either synchronously or independently around the axis of the primary radiator to steer the beam in the upper hemisphere. The resulting architecture is significantly simpler and less bulky than the typical azimuth/elevation positioner used for reflector antennas, and its profile remains unchanged while the beam is scanned. The screens needed are passive, and they do not contain reconfigurable elements. The feasibility of the scanning mechanism based on rotatable metalenses was first demonstrated in [29] by using a horn as the primary feed. More recent works have achieved higher aperture efficiency and smaller thickness by using a low-profile primary radiator [30], [31], [32], [33], [34]. The main challenge in the design of this kind of antenna for Satcom applications is the control of the grating lobes during scanning, which is strictly related to the design of the metalenses.

A similar solution is based on translating lenses: in this case, steering in elevation is achieved by the lateral translation of a thin flat lens placed a few wavelengths above a feed antenna, whereas azimuth steering is achieved by rotation of the lens or both the lens and the feed horn [35]. Dual-band operation and a beam steering range up to 50° have been demonstrated [36]. Table 3 summarizes the recent developments for antennas based on mechanical and hybrid scanning for the Ku- and Ka-bands.

## *Electronic Scanning*

Electronic beam steering antennas are the optimal solution for satellite tracking, especially when reliable and agile operation is desired. Electronic scanning is particularly advantageous for Satcom on-the-move systems (e.g., on aircraft), which require flat antennas that can rapidly repoint to the satellite to compensate for the platform motion. Fully electronic active arrays can also provide various reconfigurability characteristics, radiation pattern shaping, wide scanning capability, multiple-beam generation, and power sharing among beams through distributed amplification.

Despite the extended capabilities offered by phased arrays, the high cost and complexity of such antennas have, for a long time, limited their widespread use in commercial systems. For this reason, several approaches have been proposed to realize cost-effective electronic scanning antennas, including tunable reflectarrays and transmitarrays [36], [37], [38], [39], [41] and liquid crystal-based antennas [42], [43]. However, the typical components used for tuning the elements, such as p-i-n and varactor diodes, microelectromechanical systems, and liquid crystals, are associated with increased dissipation losses.

Recent developments of electronic chipsets with lower cost and higher power (see the "Beamformers" section) have significantly contributed to renewed interest in active array antennas. More specifically, the cost of fully active phased arrays has recently dropped thanks to the advancement of Si multichannel chips to be used for Tx/Rx modules [44], [45], [46], [47], [48], [49], [50], [51], [52], [53], [54], [55], [56], [57], [58], paving the

way to the realization of the Satcom phased arrays that are now commercially available.

Recent literature reports the performance of numerous Ku- and Ka-band phased arrays. A comparison between the measured effective isotropic radiated power (EIRP) and G/T for the Tx and Rx cases, respectively, of different prototypes is reported in Table 4. Regarding the scanning capability, the need for terminal antennas able to scan to larger angles is emerging to guarantee agile connections to different satellites. However, conventional planar phased-array antennas exhibit limitations when steering a pencil beam over a large field of view. The first is the deterioration of the antenna active reflection coefficient when scanning at low elevation. The issue is resolved with an extensive optimization process of the radiating elements and the array lattice and with the help of matching layers. However, even when good matching is achieved for wide scan angles, the diminished aperture projection (proportional to $\cos\theta$, where $\theta$ is the scan angle) translates into a reduced antenna gain. For this reason, a tradeoff is in order among the use of conformal and multipanel arrays [59], curved radomes that increase the scan range [60], [61], [62], [63], and a combination of electronic scanning with a small mechanical tilt.

Another known limitation of current Satcom phased arrays is the narrow bandwidth that forces the use of multiple antennas to cover different frequency bands. In applications that require a terminal mounted on a mobile platform, the space available is often limited, and the presence of two antennas is a major drawback. In this regard, it may be beneficial to use a wideband array simultaneously covering multiple bands [64], [65], [66]. This solution may reduce the volume and costs of the system, including fuel costs created by the weight and drag from the antennas. Note that, in wideband arrays, the isolation between different bands and Tx and Rx channels is a further difficulty that makes the design cumbersome.

**TABLE 3. A comparison of reported Ku- and Ka-band Tx and Rx mechanical and hybrid solutions.**

| Tx | Frequency Band (GHz) | Technology | Polarization | Scan Range | | EIRP (dBW) | Gain (dBi) | Maximum Scan Loss (dB) | Aperture (cm)/ Thickness (cm) |
|---|---|---|---|---|---|---|---|---|---|
| | | | | Azimuth | Elevation | | | | |
| [27] | 13.75–14.5 (Ku) | Rotatable VICTS | Tracking linear | 360° | 7.5–90° | 57.5 (PSat) | 38* | 4.5 | 75 (diameter)*/10.7 |
| [9] | 14–14.5 (Ku) | Hybrid phased array | Tracking linear | 360° | 15–75° (16 beams) | — | 36 | 4 | 64 × 19.2/22.5 |
| [28] | 27.5–31 (Ka) | VICTS | Switchable circular | 360° | 7.5–90° | 55.5 | 38* | 4.5 | 43.2 (diameter)/9.1 |
| [36] | 30 (Ka) | Translating lenses | Circular | 360° | 50–90° | — | 27 | 3.3 | 11.9 × 11.9/12 |
| **Rx** | **Frequency Band (GHz)** | **Technology** | **Polarization** | **Scan Range** | | **G/T (dB/K)** | **Peak Gain (dBi)** | **Maximum Scan Loss (dB)** | **Size (cm)/ Thickness (cm)** |
| | | | | **Azimuth** | **Elevation** | | | | |
| [27] | 10.7–12.75 (Ku) | Rotatable VICTS | Tracking linear | 360° | 7.5–90° | 18.5 (peak) | 39* | 4.5 | 75 (diameter)*/10.7 |
| [9] | 12.25–12.75 (Ku) | Hybrid phased array | Tracking linear | 360° | 15–75° | — | 35 | 4 | 64 × 19.2/22.5 |
| [10] | 11.57–11.85 (Ku) | Hybrid phased array | Circular | 360° | 15–55° | 10 | 31.5 | <3 | 80 (diameter)/13.5 |
| [30] | 11 (Ku) | Rotatable lenses | Single linear | 360° | 39–90° | — | 19.4 | 3 | 16.35 × 16.35/3.5 |
| [32] | 12.5 (Ku) | Rotatable lenses | Dual linear | 360° | 50–90° | — | 17.8 | 3 | 12.38 × 12.38/2.8 |
| [28] | 17.8–21.2 (Ka) | Rotatable VICTS | Switchable circular | 360° | 7.5–90° | 18.5 | 40.5* | 5 | 63.5 (diameter)/9.1 |
| [36] | 20 (Ka) | Translating lenses | Circular | 360° | 50–90° | — | 24 | 3.6 | 11.9 × 11.9/12 |

dBi: decibel isotropic; PSat: saturated output power.
*Estimated from data sheets.

## Beamformers

Beamforming may be achieved in many ways, with performance that may change considerably if complexity, flexibility, and costs are considered. In this article, we review three main classes of beamforming:

1) analog circuit-based passive beamforming with a limited number of orthogonal beams
2) analog active beamforming based on highly integrated Si beamformers, implementing phased-array functionalities.
3) DBF.

### *Analog Circuit-Based Passive Beamforming*

Analog circuit-based beamforming solutions are typically well adapted for array antennas with a moderate size and a limited number of beams, typically a single beam and maybe two for user segment applications requiring a make-before-break handover [67]. These are of interest for LEO constellation systems with medium-gain requirements, such as Internet of Things terminals, where a conventional analog beamforming network may be an acceptable solution in terms of complexity and performance. Over recent years, there has been a resurgence of interest for analog solutions based on orthogonal beamforming networks [68]. Most studies are based on the well-known Butler matrix [69], [70], [71], [72], and some also consider the less-known Nolen matrix [73], [74], [75], [76]. A general form of a parallel orthogonal beamforming network for single-layer implementation has also been recently proposed [77], as beamforming theory is still an active field of research. A comparison of these different beamforming matrices is provided in Table 5. Most papers focus on practical implementations, with particular interest in millimeter-wave designs and, more specifically, 5G terrestrial communications enabling interesting synergies with Satcom in the Ku- and Ka-bands. Solutions based on low-cost substrate-integrated waveguide technology [78] are particularly appealing for applications that require cheap mass-produced terminals, such as maritime transport asset tracking.

Orthogonal beamforming matrices have the advantage of producing multiple beams while avoiding recombination losses inherent to standard corporate networks [68]. These are generally used in a beam-switching configuration and in simultaneous multiple fixed-beam operation, although some works have explored the capability they offer to combine beam switching and beam steering [79], [80], [81]. Because their complexity generally increases exponentially with the number of beams, most designs reported are limited to 4 × 4 and 8 × 8 matrices, with some rare examples of 16 × 16 Butler matrices [82], [83], [84]. For larger arrays, a hybrid beamforming approach implementing typically analog beamforming at the subarray and tile level and DBF at the array level is considered a promising approach to combine the benefits and mitigate the drawbacks of both technologies [85], [86]. Compared to a fully digital implementation, the hybrid

**TABLE 4. A comparison of reported Ku- and Ka-band Tx and Rx phased arrays.**

| Tx | Frequency Band (GHz) | Antenna Elements | Number of Elements | Polarization | Scan Range | Maximum EIRP (dBW) at P1dB | Scan Loss at Maximum Scan Angle (dB) | Aperture Size (cm²) |
|---|---|---|---|---|---|---|---|---|
| [46] | 12–14.5 (Ku) | Stacked patches | 4 × 4 | Dual | ±40° | 7.5 at 12.5 GHz | ≈ 3 | 10 × 7 |
| [47] | 13–14.6 (Ku) | Stacked patches | 16 × 16 | Dual | ±60° | 34 at 14 GHz | ≈ 5 | 17 × 17 |
| [48] | 14–14.5 (Ku) | Stacked patches | 32 × 32 | Dual | ±75° | 44 at 14.25 GHz | ≈ 7 | 28.9 × 33.2 |
| [50] | 29.5–30 (Ka) | Stacked patches | 32 × 32 | Dual | ±60° | 44 at 29.7 GHz | ≈ 4.5 | 16 × 16 |
| [51] | 27.5–31 (Ka) | Patches | 16 × 16 | Single | ±70° | 34.5 at 30 GHz | ≈ 4 | ≈ 8 × 8 |
| [52] | 26.5–29.5 (Ka) | Patches | 8 × 8 | Dual | ±50° | 24 at 28 GHz | ≈ 5 | 7 × 7 |

| Rx | Frequency Band (GHz) | Antenna Elements | Number of Elements | Polarization | Scan Range | G/T (dB/K) | Scan Loss at Maximum Scan Angle (dB) | Aperture Size (cm²) |
|---|---|---|---|---|---|---|---|---|
| [51] | 27.5–31 (Ka) | Patches | 16 × 16 | Single | ±70° | –1 | ≈ 4 | ≈ 8 × 8 |
| [54] | 11.7–12.2 (Ku) | Patches | 94 | Dual | ±60° | 0.9 | ≈ 4.1 | 24 × 25 |
| [55] | 10.6–12.5 (Ku) | Patches | 16 × 16 | Dual | ±70° | 5.4 | ≈ 5–8 | 22.2 × 19.7 |
| [56] | 10.9–12.6 (Ku) | Stacked patches | 156 | Dual | ±70° | 0.3 | ≈ 7.4 | $\pi(11)^2$ |
| [58] | 10.7–12.7 (Ku) | Patches | 32 × 32 | Dual | ±70° | 10.5 | ≈ 8 | 39 × 34 |

P1db: 1 dB compression point.

beamforming antenna system also has $N$ radiating elements but only $N/N_s$ RF chains, where $N_s$ is the number of elements per subarray, instead of $N$ on the fully DBF antenna system. The subarrays may be fixed and reconfigurable, possibly including amplitude and phase control in a fully reconfigurable design. The analog part may be further extended to have multiple inputs and multiple outputs, with one RF chain per input port. Using orthogonal beamforming matrices in the analog part enables a more efficient design, at the expense of scanning range restrictions.

### Analog Active Beamforming

Beamforming integrated circuits (ICs) interface the antenna elements and beam-splitting/combining networks. On Tx, their role is to map input signals to multiple outputs with specific gain and phase coefficients that correspond to the specific position of the antenna element. In the Rx direction, the functional role is reversed, and in addition, an adequate low NF is needed to guarantee the required G/T since, in most of the active Satcom arrays, the beamforming IC is interfacing directly with the radiating elements without an external LNA. Today, there is a range of commercial off-the-shelf (COTS) beamforming ICs available in the market, covering *X*, Ku-, Ka-, and even Q/V bands. They come in various configurations, e.g., in multichannel architectures, where, for instance, four inputs are mapped to four outputs, i.e., containing 16 amplitude and phase control nodes [87]. Other configurations incorporate the signal combining and splitting functions [88] and even the down-converting functions to enable beamforming at the digital level [89]. Unlike 5G beamforming, Satcom active antennas have larger apertures and use a larger communication bandwidth, and hence, beam squint effects need to be considered. For this reason, the beamforming IC should cover the necessary delay to compensate for dispersion across the antenna aperture.

Low dc power, often referred per single beamforming node, is also of very high importance, as beamforming ICs contribute significantly to overall power consumption of the active array. Low-power beamforming ICs available in the market today consume less than 10 mW per beamforming node, but they have a 1 dB compression point (P1dB) of less than 0 dBm. Consequently, an additional output amplification is used to reach the output power level required by Satcom links. The main contribution determining the power consumption comes from the on-chip gain blocks that compensate the splitting losses and losses of amplitude/phase/time delay control blocks. The losses of these elements are minimized through an accurate choice of the beamforming architecture and the integration technologies. As an example, the losses of transmission lines can be reduced by design techniques, such as the thin-film microstrip that shields the line from lossy low-resistivity Si substrates in Si–germanium (SiGe) bipolar CMOS (BiCMOS) implementations.

As far as Si-on-insulator (SOI) technologies are concerned, the inherent physical properties of the insulator will offer higher isolation between channels and low-loss implementation of switching functions and high-Q inductors allowing superior performance. This is evident looking at the NF performance. SOI 22- and 45-nm nodes have recently demonstrated an NF below 1.5 dB, approaching the state-of-art levels obtained in gallium arsenide (GaAs) [90]. On the other hand, considering the P1dB required by Satcom applications, SiGe BiCMOS with higher voltage breakdown levels will outperform RF-SOI amplifiers by several decibels. Furthermore, SiGe performance is achieved without applying transistor stacking techniques, and it avoids the risks associated with the time-dependent dielectric breakdown, which is known to be one of the most important degradation mechanisms affecting the reliability of CMOS devices [91].

**TABLE 5. A comparison of analog beamforming matrices with *M* input ports and *N* output ports.**

| Matrix Type | Design Examples | Number of Beams | Number of Couplers | Number of Phase Shifters | Number of Crossovers | Frequency Response | Design Implementation |
|---|---|---|---|---|---|---|---|
| Butler matrix* | [70], [71], [72] | $M = 2n$ | $nN/2$ | $(n - 1)N/2$ | $(N - n - 1)$ $N/2$ | Broadband to wideband | Preferably dual layer |
| Serial Nolen matrix | [74] | $M \leq N$ | $M(2N - M - 1)/2$ | $M(2N - M - 1)/2$ | Zero | Narrow band | Very compact single layer |
| Parallel Nolen matrix | [75], [76] | $M = N$ | $N(N - 1)/2$ | $N(N - 1)/2$ | Zero | Broadband | Single layer |
| Generalized parallel matrix | [77] | $M = N$ | $N(N - 1)/2$ | $N(N - 1)/2$ | Zero | Broadband | Compact single layer |

*Assuming a standard form with four-port couplers as building blocks, $N = 2^n$.

The availability of wafer-level packaging solutions for a given technology is another important aspect to consider to facilitate array assembly and allow for proper thermal management, which is a particular challenge for SOI. Suitable wafer-level packaging techniques advance rapidly together with semiconductor processes, and, for instance, the maturity of wafer-level packaging, such as the embedded wafer-level ball grid array, has also been proved at millimeter-wave frequencies [92], [93].

### *DBF*

LEO constellations are predicted to deliver high-throughput broadband and ubiquitous services with low latency. The envisioned scenario, however, will necessitate that the user terminal tracks multiple satellites simultaneously in terms of position as well as polarization to provide truly uninterrupted operation. Although analog beamformers offer the unparalleled capability to realize single-beam phased-array antennas with low hardware complexity and power consumption, analog beam steering poses severe challenges when designing point-to-multipoint antenna systems. In particular, for higher operating frequencies in the micro- and millimeter-wave regimes, spatial multiplexing systems based on analog beamformers commonly suffer from inherent space constraints because the amount of analog circuitry is inevitably linked with the number of independent beams. In contrast, multibeam antenna systems using DBF do not show these limitations, as they perform the namesake function solely in the digital back end [94]. This leads to a simplified RF chain per antenna element, basically constituting an amplification and frequency conversion stage for Tx and Rx, respectively. DBF processing on the element-level has the highest degree of flexibility in synthesizing multiple beams simultaneously because the Tx and Rx signals at each antenna element can be arbitrarily manipulated, duplicated, and combined in the digital domain, hence avoiding signal-to-noise ratio (SNR) degradation. Furthermore, unlike their analog counterparts, fully digital beamformer processors can seamlessly apply frequency-dependent amplitude tapering and phase shifting enhanced by the possible compensation of hardware impairments through channel-level equalization, in-phase/quadrature balancing, and static local oscillator phase offsets at each antenna element [95].

Pushed by the ambitious data throughput goals of near-future LEO/medium Earth orbit Satcom, DBF-based antenna terminals are becoming an interesting design approach to cover large instantaneous bandwidths while avoiding the use of analog true-time delay elements [96]. Despite all these advantages, the implementation effort of the signal processing back end strongly scales with the number of antenna elements as well as the system bandwidth [97]. Ahead of their time, the first DBF antenna modules for mobile Satcom terminals at 30 GHz have been presented in [98] and [99]. In these pioneering works, the digital baseband processing unit supports the control of up to 64 radiation elements within a signal bandwidth of a few tens of megahertz. In a situation radically different from 10 years ago, when the use of COTS components ruled active antenna design, the custom development of application-specific ICs (ASICs) for specific commercial sensor and communication applications has become very much mainstream now. An example for the current generation of DBF ASICs for the Satcom market segment is SatixFy's Prime [100]. The true-time delay DBF chip supports up to 32 antenna elements and can be connected with other chips to span large antenna apertures. The individual signals at each antenna element are translated between the analog and digital domain by high-speed analog-to-digital converters (ADCs) and digital-to-analog converters, respectively.

Apart from high-resolution digital phase shifters and digital delay circuits, the signal processing inside beamformer ASICs may also correct RF front-end imperfections, enabling wideband signal transmission and reception across 1 GHz of bandwidth in single-beam mode. The enormous advances in CMOS semiconductor technologies have also enabled the commercial realization of data converters for direct RF sampling up to the Ka-band [101]. The latest trends show that digital beamformer ASICs enhanced by direct sampling up to the Ka-band are going to be deployed in future satellite payloads and thus circumvent the need for frequency conversion stages [102]. Although this all-in-one DBF technology is not yet competitive to be used on the element level in mobile DBF antenna terminals, the availability of high-performance data converters has paved the way for new code-based beamforming architectures. In [103], more specifically, a code division multiplexing technique has been proposed to aggregate the individual signals from the antenna elements at the analog RF front end into a single ADC. Compared to conventional DBF techniques, a remarkable reduction of the number of required ADCs has been demonstrated, which, in return, must feature a higher sampling rate and analog bandwidth.

## Semiconductor Technologies

The integration level offered by monolithic microwave ICs (MMICs) is a key feature of LEO constellations. Integration processes have advanced considerably, making possible the design of complete systems on chip in the frequency band considered in this review (i.e., the Ku-/Ka-bands). In this scenario, four main

semiconductor families appear to be attractive candidates for the aimed-at frequency bands and performance: 1) GaAs, 2) Ga nitride (GaN), 3) SiGe, and 4) Si. The two former technologies belong to the wide-bandgap semiconductor family, which intrinsically leads to greater output power and a reduced NF. On the other hand, Si- and SiGe-based technologies present reduced footprints, higher gains, and the possibility of integrating digital control circuitry in a single die together with RF functions.

Considering power and bandwidth, GaN really emerges as the winner when compared with the competing technologies. In fact, progress in GaN device technology is considered crucial to the viability of power amplification in space and other critical applications in the future. In the past decade, GaN MMICs and discrete GaN devices have significantly improved their efficiency, power density, reliability, and overall output power. In the frequency bands considered in this review, the Ku- and Ka-bands, GaN-based devices and circuits have already demonstrated superior performance in all these figures of merit while simplifying MMIC architectures and minimizing the overall product footprint. Nevertheless, GaN-based MMICs are undergoing further research and development efforts accompanied by considerable investments to improve efficiency, output power, manufacturing processes, and module packaging. Note that prepackaged devices and carriers are still being employed as the most convenient and cost-effective means of building high-power solid-state PAs for lower frequencies, typically below 30 GHz. As far as GaAs is considered, this technology offers the nonnegligible advantage of lower noise and an ability to integrate with CMOS technologies. Also, GaAs allows for the design of complete core chips that integrate into Tx/Rx modules.

The second family, 3) and 4) in the preceding list, is Si based. SiGe offers heterojunction bipolar transistors (HBTs) in addition to MOSFETs [104]. Even though MOSFETs integrated in a 130-nm process can comfortably address the Ku-/Ka-bands with respectable performance, HBTs offer much better performance, usually with the drawback of a more expensive technology. Modern pure Si technologies offer additional features, such as SOI substrates that have effectively pushed forward the performance of these technologies, especially in terms of the NF [105], as reported later in the article.

The choice among the technologies briefly described up to now is usually driven by four principal drivers: the power output, NF, footprint, and cost. The first two drivers determine the performance of a satellite terminal and the quality of the link in terms of the availability and data rate. For this reason, in the succeeding sections, the state of the art of PAs and LNAs will be overviewed in greater detail. The footprint of the device directly affects the level of integration achievable. The area of the devices is a critical parameter affecting the realization of electronically scanned antennas and phased arrays. In fact, phased arrays require that the distance between radiating elements be less than half of a wavelength. The last driver, cost, is probably the most difficult to evaluate, and it will be only marginally considered. In fact, technology selection involves a complex tradeoff among variables that affect cost, such as the technology type and node, volume, expected circuit complexity (~die area), production wafer size, and process availability (i.e., the wafer fabrication process time).

Costs are critical in terminals that adopt phased-array antennas because of the number of components. In these cases, Si-based technologies are the ones that offer the best level of integration. Si technologies have one principal cost factor in nonrecurring costs, mainly related to the mask set. In the case of RF-SOI technology, nonrecurring costs are absorbed only under a large production volume, while for SiGe, nonrecurring costs could be several times lower than those of advanced SOI nodes (e.g., 130-nm SiGe versus advanced RF-SOI). It is evident that SiGe will make sense in Satcom communications, where lower volume and high-end RF performance (e.g., a higher linearity, higher P1dB, and lower NF) are required. Several foundries have recently improved this tradeoff for SiGe BiCMOS by moving from 200- to 300-mm wafers, enhancing production efficiency and making SiGe suitable even for a large market above the Ku-band. The indicative tradeoff for SiGe and RF-SOI technologies is presented in Table 6.

### PAs

The design of RF PAs focuses on increasing the output power and optimizing the dc-to-RF efficiency. Consequently, benchmarking a PA's saturation power ($P_{sat}$) and its power-added efficiency (PAE) provides a straightforward way to determine its performance. Figure 2 includes a scatter plot of the current state-of-the-art PAs, comparing their PAE versus their. In applications involving high-data-rate communication using higher-level modulation methods, other factors, such as linearity and the noise–power ratio, intervene to determine an efficient and robust communication link versus their PAE. Figure 2 shows a clear separation between III-V technologies (i.e., GaAs and GaN) and Si technologies, symbolically delimited by the 30-dBm barrier due to the difference in operating voltage between III-V and Si-based technologies. PAs of the III-V group require a voltage around 12–28 V, while Si amplifiers need a voltage between 1 and 4 V.

GaN appears to be a superior candidate for the design of PAs when compared to GaAs and is becoming the

**TABLE 6. The indicative tradeoff for three selected processes adopted in most beamforming ICs: two RF-SOI technology nodes and SiGe BiCMOS.**

| Technology | Nonrecurring Cost | Cost/Area for Amplifier | Wafer Process Time | Integration Density | Thermal Management | Voltage Breakdown | P1dB | PAE | NF |
|---|---|---|---|---|---|---|---|---|---|
| RF-SOI for millimeter-waves | Baseline | | ~8–12 weeks | ••• | • | • | • | •• | ••• |
| RF-SOI for Ku-and Ka-bands | <1/2 of baseline | Baseline | ~8–12 weeks | •• | • | •• | •• | •• | ••• |
| SiGe BiCMOS | ~1/10 of baseline | 2× baseline | ~10–15 weeks | • | ••• | ••• | ••• | ••• | •• |

technology of choice across frequency bands and markets. GaN amplifiers present a $P_{sat}$ in the 36–46 -dBm range [106], [107], [108], [109], [110], [111], [112], while their GaAs counterparts are within the 34–40-dBm range [111], [112], [113], [114], [115], [116]. In addition, GaN PAs also show a superior PAE, which can surpass 40%, while GaAs PAs present PAEs of the order of 30%. Initially, higher output power and smaller form factors were the focus of GaN product development. However, the resulting thermal constraints at the system level push R&D efforts to achieve a better balance with efficiency to help reduce dissipated power and ease the thermal load at the system level.

In Si-only technologies, output powers of around 23 dBm have been reached [117] in Doherty-based PAs. On the other hand, with single-ended architectures that do not rely on power-combining techniques, most Si-based technologies tend to offer $P_{sat}$ levels in the 14–20-dBm level [118], [119], [120], [121], [122], [123], [124]. In turn, at these frequencies, these technologies tend to report PAE levels in the 20%–45% range [117], [118], [119], [120], [121], [122], [123], [124]. Finally, concerning the linearity of Si-based PAs, they tend to show output 1-dB compression points of around 1 to 1.5 dB below the $P_{sat}$ [117], [118], [119], [120], [121], [122], [123], [124].

On the other hand, SiGe technologies, with their HBT transistors, feature a $P_{sat}$ in the 17–23-dBm range [125]–[129] associated with PAE levels of around 30%–43%. Note that, compared to III-V technologies, the differences of the performance of PAs in pure Si and SiGe technologies is not sufficient to determine the choice of a given technology in this band. A clearer difference appears when operating frequencies move to greater ranges, where the performance of SiGe HBTs clearly surpasses that of Si-based MOSFETs.

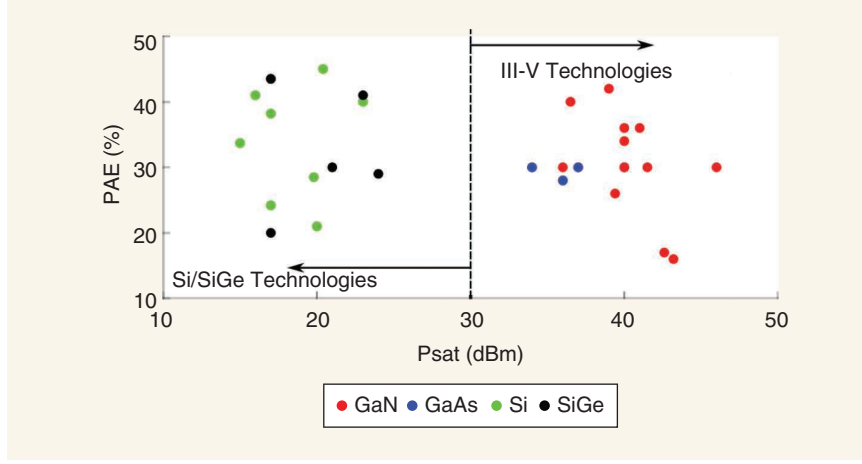


**Figure 2.** *The PAE versus the $P_{sat}$ of current state-of-the-art GaN [106], [107], [108], [109], [110], [111], [112], GaN [111], [116], Si [117], [118], [119], [120], [121], [122], [123], [124], and SiGe PAs [125], [126], [127], [128], [129] in the Ku/Ka frequency bands.*

## LNAs

The LNA is employed in satellite application front-end receivers to amplify the degraded RF signals captured by the antenna to the desired level. The LNA boosts the received signal power by adding minimal noise and distortion to mitigate the impact of noise added by the components of the RF receiver chain. Its effect is to improve the SNR, which is essential for the quality of the radio link. Design requirements combine the minimum NF with the high gain and pose severe challenges to the designer. The complexity of the design further increases if one considers the problems of impedance matching, low power consumption, linearity, and stability.

Figure 3 presents the NF versus the gain of current state-of-the-art GaAs [111], [112], GaN [111], [112], SiGe [131], [132], [133], [134], [135], [136], [137], [138], and Si [130], [139], [140], [141], [142], [143], [144], [145] LNAs

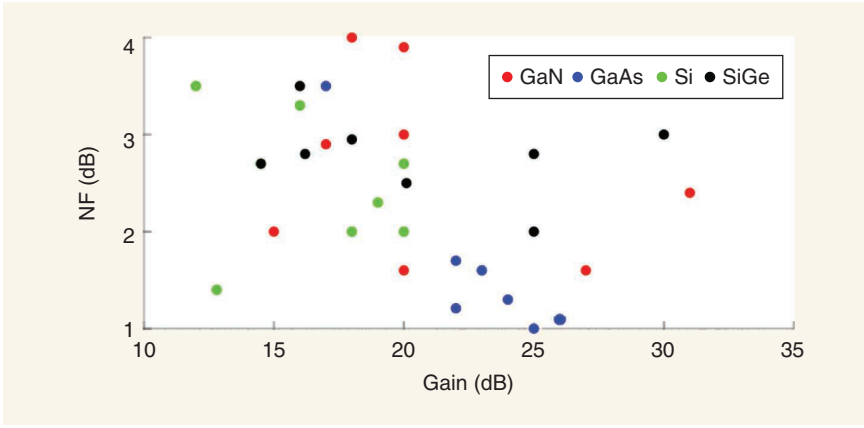


**Figure 3.** *The NF versus the gain of current state-of-the-art GaAs [111], [112], GaN [111], [112], SiGe [131], [132], [133], [134], [135], [136], [137], [138], and Si [130], [139], [140], [141], [142], [143], [144], [145] LNAs in the Ku/Ka frequency bands.*

in the Ka/Ku frequency bands. LNAs based on GaAs dominate the low-NF part of the plot, followed by GaN devices. Note that low-NF LNAs can also be built with SOI platforms [130]. High-gain LNAs are achievable with SiGe and GaN processes, as well. GaN LNAs ensure good RF performance under low dc power consumption, which is a fundamental requirement for space and ground segments [40]. The latter is often achieved by reducing the nominal bias point to operate GaN HEMTs in low-current-density areas.

Concerning Si- and SiGe-based technologies, SiGe is more suited for the design of high-gain LNAs, while pure Si-based processes offer a better NF thanks to the SOI technology. LNAs with 30-dB-gain LNAs realized with a 0.13-$\mu$m BiCMOS process have been reported [131]. SiGe LNAs present an NF in the 2–3-dB range in the Ka-/Ku-bands, with gains that span the 15–30-dB range [131], [132], [133], [134], [135], [136], [137], [138]. Si-based LNAs present more modest gain levels in the 12–20-dB range but show NFs close to those of GaAs (i.e., nearly 1 dB) up to 3.5 dB [130], [139], [140], [141], [142], [143], [144], [145].

LNA performance is not limited only by the intrinsic gain and NF of a given transistor in a technology. The NF is largely impacted by the matching network required to adapt the input/output impedance of the transistor to 50 Ω, typically. Hence, the quality factor of passive devices in a certain technology will greatly limit the performance of an LNA. Moreover, other parameters should be considered. For instance, LNAs are known for being particularly sensitive to high-power RF inputs that can put them into breakdown mode. Among the considered technologies, GaN can withstand the greatest amounts of power without entering a breakdown regime, followed by GaAs and SiGe, in that order. Recently, there were reports of GaN LNAs surviving input power levels over 30 dBm in a continuous wave and nearly 50 dBm in pulse conditions. Moreover, GaN LNAs demonstrated high linearity with third-order output intermodulation points around 40 dBm [146]. Electrostatic discharge (ESD) events can also present a threat for most LNAs. For this reason, ESD must be carefully studied. Note that extra circuitry must be added to protect the LNA against ESD events, which can degrade the performance of the circuit. Hence, choosing a technology that is more resilient against ESD events may not only ease the design of an LNA but also dictate the choice between two technologies. For instance, SiGe LNAs have appeared to be more robust against this kind of event than GaAs LNAs [40].

## Conclusions

The present review provided a general outline of the current technologies for satellite user terminals. Even though the technologies reported are common to GEO and LEO applications, the focus was on the former case. Starting from the antenna, the review covered the various components of a user terminal, including the antenna, beamforming network, and LNAs and PAs. Comparative tables were provided for the reader to get a quick overview of the available technologies. The presented material is suitable for researchers seeking an overview of the current state of the art in the field. It is the authors' hope that the article will prove useful to researchers and engineers working in the field.

## References

[1] I. del Portillo, B. G. Cameron, and E. F. Crawley, "A technical comparison of three low earth orbit satellite constellation systems to provide global broadband," *Acta Astronautica*, vol. 159, pp. 123–135, Jun. 2019, doi: 10.1016/j.actaastro.2019.03.040.

[2] N. Pachler, I. del Portillo, E. F. Crawley, and B. G. Cameron, "An updated comparison of four low earth orbit satellite constellation systems to provide global broadband," in *Proc. 2021 IEEE Int. Conf. Commun. Workshops (ICC Workshops)*, pp. 1–7, doi: 10.1109/ICCWorkshops50388.2021.9473799.

[3] "Exhibit 1 supplemental information regarding earth stations." SpaceX. Accessed: May, 2021. [Online]. Available: https://apps.fcc.gov/els/GetAtt.html?id=197812&x=

[4] *SatMaster Pro MK10.4d*, Arrow Technical Services, U.K., 2020.

[5] "MPT™ – Multi-purpose terminal: Airborne stabilized VSAT system." Orbit. Accessed: May 2020. [Online]. Available: https://orbit-cs.com/wp-content/uploads/2021/08/Orbit-MPT-DS-v0.03.pdf

[6] "G-18L Ku-/Ka-band antenna: Hybrid satellite antenna for mobility." Viasat. [Online]. Accessed: May 2020. Available: https://www.viasat.com/content/dam/us-site/antenna-systems/documents/1229461_G-18L_KuKa_Datasheet_006_web.pdf

[7] "KuKarray-2L antenna: Hybrid Ka-band/Ku-band satellite antenna for mobility." Viasat. Accessed: May 2020. [Online]. Available: https://www.viasat.com/content/dam/us-site/antenna-systems/documents/1229461_KuKarray2L_Datasheet_005_web.pdf

[8] F. Tiezzi, S. Vaccaro, D. Llorens, C. Dominguez, and M. Fajardo, "Ku-band hybrid phased array antennas for mobile satellite communication systems," in *Proc. 2013 7th Eur. Conf. Antennas Propag. (EuCAP)*, pp. 1605–1608.

[9] G. Han, B. Du, W. Wu, and B. Yang, "A novel hybrid phased array antenna for satellite communication on-the-move in Ku-band," *IEEE Trans. Antennas Propag.*, vol. 63, no. 4, pp. 1375–1383, Apr. 2015, doi: 10.1109/TAP.2015.2389951.

[10] R. Vincenti Gatti, L. Marcaccioli, E. Sbarra, and R. Sorrentino, "Flat array antenna for Ku-band mobile satellite terminals," in *Proc. 5th Eur. Conf. Antennas Propag. (EUCAP)*, 2011, pp. 2618–2622.

[11] T. Ströber, S. Tubau, E. Girard, H. Legay, G. Goussetis, and M. Ettorre, "Shaped parallel-plate lens for mechanical wide-angle beam steering," *IEEE Trans. Antennas Propag.*, vol. 69, no. 12, pp. 8158–8169, Dec. 2021, doi: 10.1109/TAP.2021.3090789.

[12] M. Śmierzchalski et al., "A novel dual-polarized continuous transverse stub antenna based on corrugated waveguides—Part I: Principle of operation and design," *IEEE Trans. Antennas Propag.*, vol. 69, no. 3, pp. 1302–1312, Mar. 2021, doi: 10.1109/TAP.2020.3028236.

[13] M. Śmierzchalski et al., "A novel dual-polarized continuous transverse stub antenna based on corrugated waveguides—Part II: Experimental demonstration," *IEEE Trans. Antennas Propag.*, vol. 69, no. 3, pp. 1313–1323, Mar. 2021, doi: 10.1109/TAP.2020.3037809.

[14] N. T. Nguyen, R. Sauleau, M. Ettorre, and L. L. Coq, "Focal array fed dielectric lenses: An attractive solution for beam reconfiguration at millimeter waves," *IEEE Trans. Antennas Propag.*, vol. 59, no. 6, pp. 2152–2159, Jun. 2011, doi: 10.1109/TAP.2011.2144550.

[15] A. D. Greenwood and J. Jian-Ming, "A field picture of wave propagation in inhomogeneous dielectric lenses," *IEEE Antennas Propag. Mag.*, vol. 41, no. 5, pp. 9–18, Oct. 1999, doi: 10.1109/74.801510.

[16] J. Thornton, D. Smith, S. J. Foti, and Y. Y. Jiang, "Reduced height Luneburg lens antennas for satellite communications-on-the-move," in *Proc. 2015 Conf. Microw. Techn. (COMITE)*, pp. 1–4, doi: 10.1109/COMITE.2015.7120325.

[17] J. Pendry, D. Schurig, and D. Smith, "Controlling electromagnetic fields," *Science*, vol. 312, no. 5781, pp. 1780–1782, Jun. 2006, doi: 10.1126/science.1125907.

[18] Y. Su and Z. N. Chen, "A flat dual-polarized transformation-optics beamscanning Luneburg lens antenna using PCB-stacked gradient index metamaterials," *IEEE Trans. Antennas Propag.*, vol. 66, no. 10, pp. 5088–5097, Oct. 2018, doi: 10.1109/TAP.2018.2858209.

[19] C. Mateo-Segura, A. Dyke, H. Dyke, S. Haq, and Y. Hao, "Flat Luneburg lens via transformation optics for directive antenna applications," *IEEE Trans. Antennas Propag.*, vol. 62, no. 4, pp. 1945–1953, Apr. 2014, doi: 10.1109/TAP.2014.2302004.

[20] Y. J. Park, A. Herschlein, and W. Wiesbeck, "A photonic bandgap (PBG) structure for guiding and suppressing surface waves in millimeter-wave antennas," *IEEE Trans. Microw. Theory Techn.*, vol. 49, no. 10, pp. 1854–1859, Oct. 2001, doi: 10.1109/22.954798.

[21] L. Xue and V. F. Fusco, "Printed holey plate Luneburg lens," *Microw. Opt. Technol. Lett.*, vol. 50, no. 2, pp. 378–380, Feb. 2008, doi: 10.1002/mop.23087.

[22] C. Pfeiffer and A. Grbic, "A printed, broadband Luneburg lens antenna," *IEEE Trans. Antennas Propag.*, vol. 58, no. 9, pp. 3055–3059, Sep. 2010, doi: 10.1109/TAP.2010.2052582.

[23] M. Huang, S. Yang, F. Gao, R. Quarfoth, and D. Sievenpiper, "A 2-D multibeam half Maxwell fish-eye lens antenna using high impedance surfaces," *IEEE Antennas Wireless Propag. Lett.*, vol. 13, pp. 365–368, Feb. 2014, doi: 10.1109/LAWP.2014.2306207.

[24] O. Quevedo-Teruel, J. Miao, M. Mattsson, A. Algaba-Brazalez, M. Johansson, and L. Manholm, "Glide-symmetric fully metallic Luneburg lens for 5G communications at Ka-band," *IEEE Antennas Wireless Propag. Lett.*, vol. 17, no. 9, pp. 1588–1592, Sep. 2018, doi: 10.1109/LAWP.2018.2856371.

[25] H. Lu, Z. Liu, Y. Liu, H. Ni, and X. Lv, "Compact air-filled Luneburg lens antennas based on almost-parallel plate waveguide loaded with equal-sized metallic posts," *IEEE Trans. Antennas Propag.*, vol. 67, no. 11, pp. 6829–6838, Nov. 2019, doi: 10.1109/TAP.2019.2927862.

[26] Q. Liao, N. J. G. Fonseca, and O. Quevedo-Teruel, "Compact multibeam fully metallic geodesic Luneburg lens antenna based on non-Euclidean transformation optics," *IEEE Trans. Antennas Propag.*, vol. 66, no. 12, pp. 7383–7388, Dec. 2018, doi: 10.1109/TAP.2018.2872766.

[27] "ThinAir® Ku3030: Ku-band SATCOM antenna for global in-flight broadband." ThinKom. Accessed: May 2020. [Online]. Available: https://www.thinkom.com/wp-content/uploads/2018/09/ku3030-datasheet_9_18_web.pdf

[28] "ThinAir® Ka2517: Ka-band SATCOM antenna for global broadband." ThinKom. Accessed: May 2021. [Online]. Available: https://www.thinkom.com/wp-content/uploads/2022/03/thinair-ka2517-datasheet.pdf

[29] N. Gagnon and A. Petosa, "Using rotatable planar phase shifting surfaces to steer a high-gain beam," *IEEE Trans. Antennas Propag.*, vol. 61, no. 6, pp. 3086–3092, Jun. 2013, doi: 10.1109/TAP.2013.2253298.

[30] M. U. Afzal and K. P. Esselle, "Steering the beam of medium-to-high gain antennas using near-field phase transformation," *IEEE Trans. Antennas Propag.*, vol. 65, no. 4, pp. 1680–1690, Apr. 2017, doi: 10.1109/TAP.2017.2670612.

[31] M. Akbari, M. Farahani, A. Ghayekhloo, S. Zarbakhsh, A. Sebak, and T. A. Denidni, "Beam tilting approaches based on phase gradient surface for mmWave antennas," *IEEE Trans. Antennas Propag.*, vol. 68, no. 6, pp. 4372–4385, Jun. 2020, doi: 10.1109/TAP.2020.2972375.

[32] H. Qiu, X.-X. Yang, Y. Yu, T. Lou, Z. Yin, and S. Gao, "Compact beam-scanning flat array based on substrate-integrated waveguide," *IEEE Trans. Antennas Propag.*, vol. 68, no. 2, pp. 882–890, Feb. 2020, doi: 10.1109/TAP.2019.2943441.

[33] Q. Zeng, Z. Xue, W. Ren, and W. Li, "Dual-band beam-scanning antenna using rotatable planar phase gradient transmitarrays," *IEEE Trans. Antennas Propag.*, vol. 68, no. 6, pp. 5021–5026, Jun. 2020, doi: 10.1109/TAP.2020.2963929.

[34] Y. Sun, F. Dang, C. Yuan, J. He, Q. Zhang, and X. Zhao, "A beam-steerable lens antenna for Ku-band high-power microwave applications," *IEEE Trans. Antennas Propag.*, vol. 68, no. 11, pp. 7580–7583, Nov. 2020, doi: 10.1109/TAP.2020.2979282.

[35] E. B. Lima et al., "Circular polarization wide-angle beam steering at Ka-band by in-plane translation of a plate lens antenna," *IEEE Trans. Antennas Propag.*, vol. 63, no. 12, pp. 5443–5455, Dec. 2015, doi: 10.1109/TAP.2015.2484419.

[36] S. A. Matos et al., "High gain dual-band beam-steering transmit array for satcom terminals at Ka-band," *IEEE Trans. Antennas Propag.*, vol. 65, no. 7, pp. 3528–3539, Jul. 2017, doi: 10.1109/TAP.2017.2702658.

[37] L. Di Palma, A. Clemente, L. Dussopt, R. Sauleau, P. Potier, and P. Pouliguen, "Circularly-polarized reconfigurable transmitarray in Ka-band with beam scanning and polarization switching capabilities," *IEEE Trans. Antennas Propag.*, vol. 65, no. 2, pp. 529–540, Feb. 2017, doi: 10.1109/TAP.2016.2633067.

[38] T. Chaloun et al., "Wide-angle scanning active transmit/receive reflectarray," *IET Microw., Antennas Propag.*, vol. 8, no. 11, pp. 811–818, Aug. 2014, doi: 10.1049/iet-map.2013.0704.

[39] P. Naseri, S. A. Matos, J. R. Costa, and C. A. Fernandes, "Phase-delay versus phase-rotation cells for circular polarization transmit arrays –application to satellite Ka-band beam steering," *IEEE Trans. Antennas Propag.*, vol. 66, no. 3, pp. 1236–1247, Mar. 2018, doi: 10.1109/TAP.2017.2787540.

[40] S.-M. Hwang and K.-H. Lee, "Comparison of ESD immunity between GaAs-based LNA and SiGe-based LNA," *IEEE Trans. Electromagn. Compat.*, vol. 54, no. 4, pp. 944–946, Aug. 2012, doi: 10.1109/TEMC.2012.2205154.

[41] A. Clemente, L. Di Palma, F. Diaby, L. Dussopt, K. Pham, and R. Sauleau, "Electronically-steerable transmitarray antennas for Ka-band," in *Proc. 13th Eur. Conf. Antennas Propag. (EuCAP)*, Krakov, Poland, 2019, pp. 1–4.

[42] R. Stevenson, M. Sazegar, A. Bily, M. Johnson, and N. Kundtz, "Metamaterial surface antenna technology: Commercialization through diffractive metamaterials and liquid crystal display manufacturing," in *Proc. 10th Int. Congr. Adv. Electromagn. Mater. Microw. Opt.*, 2016, pp. 349–351, doi: 10.1109/MetaMaterials.2016.7746395.

[43] G. Minatti et al., "Electronically reconfigurable metasurface antennas based on liquid crystal technology," in *Proc. 13th Eur. Conf. Antennas Propag.*, Krakov, Poland, 2019, pp. 1–3.

[44] G. M. Rebeiz and L. M. Paulsen, "Advances in SATCOM phased arrays using silicon technologies," in *Proc. IEEE/MTT-S Int. Microw. Symp.*, Honolulu, HI, USA, Jun. 2017, pp. 1877–1879, doi: 10.1109/MWSYM.2017.8059022.

[45] J.-C. S. Chieh, E. Yeo, M. Kerber, and R. Olsen, "Ku-band dual polarized phased array utilizing silicon beamforming chipsets," in *Proc. IEEE Topical Workshop Internet Space*, Orlando, FL, USA, May 2019, pp. 1–3, doi: 10.1109/TWIOS.2019.8724517.

[46] J.-C. S. Chieh et al., "Development of flat panel active phased array antennas using 5G silicon RFICs at Ku- and Ka-bands," *IEEE Access*, vol. 8, pp. 192,669–192,681, 2020, doi: 10.1109/ACCESS.2020.3032841.

[47] A. H. Aljuhani, T. Kanar, S. Zihir, and G. M. Rebeiz, "A scalable dual-polarized 256-element Ku-band SATCOM phased-array transmitter with 36.5 dBW EIRP per polarization," in *Proc. 48th Eur. Microw. Conf.*, Madrid, Spain, Sep. 2018, pp. 938–941, doi: 10.23919/EuMC.2018.8541746.

[48] G. Gültepe, T. Kanar, S. Zihir, and G. M. Rebeiz, "A 1024-element Ku-band SATCOM phased-array transmitter with 45-dBW single-polarization EIRP," *IEEE Trans. Microw. Theory Techn.*, vol. 69, no. 9, pp. 4157–4168, Sep. 2021, doi: 10.1109/TMTT.2021.3075678.

[49] T. Lambard, O. Lafond, M. Himdi, H. Jeuland, S. Bolioli, and L. Le Coq, "Ka-band phased array antenna for high-data-rate SATCOM," *IEEE Antennas Wireless Propag. Lett.*, vol. 11, pp. 256–259, Mar. 2012, doi: 10.1109/LAWP.2012.2189747.

[50] X. Luo et al., "A scalable Ka-band 1024-element transmit dual-circularly-polarized planar phased array for SATCOM application," *IEEE Access*, vol. 8, pp. 156,084–156,095, Aug. 2020, doi: 10.1109/ACCESS.2020.3019174.

[51] W. M. Abdel-Wahab et al., "A modular architecture for wide scan angle phased array antenna for K/Ka mobile SATCOM," in *Proc. IEEE MTT-S Int. Microw. Symp. (IMS)*, Boston, MA, USA, Jun. 2019, pp. 1076–1079, doi: 10.1109/MWSYM.2019.8700842.

[52] X. Gu et al., "Development, implementation, and characterization of a 64-element dual-polarized phased-array antenna module for 28-GHz high-speed data communications," *IEEE Trans. Microw. Theory Techn.*, vol. 67, no. 7, pp. 2975–2984, Jul. 2019, doi: 10.1109/TMTT.2019.2912819.

[53] H. Al-Saedi et al., "An integrated circularly polarized transmitter active phased-array antenna for emerging Ka-band satellite mobile terminals," *IEEE Trans. Antennas Propag.*, vol. 67, no. 8, pp. 5344–5352, Aug. 2019, doi: 10.1109/TAP.2019.2913745.

[54] I. Kaplan et al., "Electronically beam steerable antennas for broadband satellite communications," in *Proc. 8th Eur. Conf. Antennas Propag.*, The Hague, The Netherlands, Apr. 2014, pp. 2450–2454, doi: 10.1109/EuCAP.2014.6902313.

[55] A. H. Aljuhani, T. Kanar, S. Zihir, and G. M. Rebeiz, "A 256-element Ku-band polarization agile SATCOM receive phased array with wide-angle scanning and high polarization purity," *IEEE Trans. Microw. Theory Techn.*, vol. 69, no. 5, pp. 2609–2628, May 2021, doi: 10.1109/TMTT.2021.3056439.

[56] L. Baggen, S. Vaccaro, D. Llorens del Río, J. Padilla, and R. T. Sánchez, "A compact phased array for satcom applications," in *Proc. IEEE Int. Symp. Phased Array Syst. Technol.*, 2013, pp. 232–239, doi: 10.1109/ARRAY.2013.6731833.

[57] L. A. Greda and A. Dreher, "TX-terminal phased array for satellite communication at Ka-band," in *Proc. Eur. Microw. Conf.*, 2007, pp. 266–269, doi: 10.1109/EUMC.2007.4405177.

[58] G. Gültepe, T. Kanar, S. Zihir, and G. M. Rebeiz, "A 1024-element Ku-band SATCOM dual-polarized receiver with >10-dB/K G/T and embedded transmit rejection filter," *IEEE Trans. Microw. Theory Techn.*, vol. 69, no. 7, pp. 3484–3495, Jul. 2021, doi: 10.1109/TMTT.2021.3073321.

[59] A. Catalani, F. Di Paolo, M. Migliorelli, L. Russo, G. Toso, and P. Angeletti, "Ku-band hemispherical fully electronic antenna for aircraft in flight entertainment," *Int. J. Antennas Propag.*, vol. 2009, May 2009, Art. no. 230650, doi: 10.1155/2009/230650.

[60] H. Steyskal, A. Hessel, and J. Shmoys, "On the gain-versus-scan trade-offs and the phase gradient synthesis for a cylindrical dome antenna," *IEEE Trans. Antennas Propag.*, vol. 27, no. 6, pp. 825–831, Nov. 1979, doi: 10.1109/TAP.1979.1142192.

[61] H. Kawahara, H. Deguchi, M. Tsuji, and H. Shigesawa, "Design of rotational dielectric dome with linear array feed for wide-angle multibeam antenna applications," *Electron. Commun. Jpn., II Electron.*, vol. 90, no. 5, pp. 49–57, May 2007, doi: 10.1002/ecjb.20254.

[62] J. Stangel and P. Valentino, "Phased array fed lens antenna," U.S. Patent US3755815A, 1971.

[63] A. Benini et al., "Phase-gradient meta-dome for increasing grating-lobe-free scan range in phased arrays," *IEEE Trans. Antennas Propag.*, vol. 66, no. 8, pp. 3973–3982, Aug. 2018, doi: 10.1109/TAP.2018.2835575.

[64] R. J. Bolt et al., "Characterization of a dual-polarized connected-dipole array for Ku-band mobile terminals," *IEEE Trans. Antennas Propag.*, vol. 64, no. 2, pp. 591–598, Feb. 2016, doi: 10.1109/TAP.2015.2509505.

[65] A. I. Sandhu, E. Arnieri, G. Amendola, L. Boccia, E. Meniconi, and V. Ziegler, "Radiating elements for shared aperture TX/RX phased arrays at K/Ka band," *IEEE Trans. Antennas Propag.*, vol. 64, no. 6, pp. 2270–2282, Jun. 2016, doi: 10.1109/TAP.2016.2552550.

[66] A. J. van Katwijk, A. Neto, G. Toso, and D. Cavallo, "Design of wideband wide-scanning dual-polarized phased array covering simultaneously both the Ku- and the Ka-Satcom bands," in *Proc. 14th Eur. Conf. Antennas Propag.*, 2020, pp. 1–3, doi: 10.23919/EuCAP48036.2020.9135541.

[67] Y. J. Guo, M. Ansari, and N. J. G. Fonseca, "Circuit type multiple beamforming networks for antenna arrays in 5G and 6G terrestrial and non-terrestrial networks," *IEEE J. Microw.*, vol. 1, no. 3, pp. 704–722, Jul. 2021, doi: 10.1109/JMW.2021.3072873.

[68] Y. Aslan et al., "Orthogonal versus zero-forced beamforming in multibeam antenna systems: Review and challenges for future wireless networks," *IEEE J. Microw.*, vol. 1, no. 4, pp. 879–901, Oct. 2021, doi: 10.1109/JMW.2021.3109244.

[69] J. Butler and R. Lowe, "Beam-forming matrix simplifies design of electronically scanned antenna," *Electron. Des.*, vol. 9, pp. 170–173, Apr. 1961.

[70] A. A. M. Ali et al., "Design and implementation of two-layer compact wideband Butler matrices in SIW technology for Ku-band applications," *IEEE Trans. Antennas Propag.*, vol. 59, no. 2, pp. 503–512, Feb. 2011, doi: 10.1109/TAP.2010.2093499.

[71] T. Djerafi and K. Wu, "Multilayered substrate integrated waveguide 4×4 Butler matrix," *Int. J. RF Microw. Comput.-Aided Eng.*, vol. 22, no. 3, pp. 336–344, May 2012, doi: 10.1002/mmce.20602.

[72] T. Tomura et al., "A 20-GHz-band 64 × 64 hollow waveguide two-dimensional Butler matrix," *IEEE Access*, vol. 7, pp. 164,080–164,088, Nov. 2019, doi: 10.1109/ACCESS.2019.2952933.

[73] J. Nolen, "Synthesis of multiple beam networks for arbitrary illuminations," Ph.D. dissertation, Bendix Corp., Baltimore, MD, USA, Apr. 1965.

[74] N. J. G. Fonseca, "Printed S-band 4×4 Nolen matrix for multiple beam antenna applications," *IEEE Trans. Antennas Propag.*, vol. 57, no. 6, pp. 1673–1678, Jun. 2009, doi: 10.1109/TAP.2009.2019919.

[75] T. Djerafi, N. J. G. Fonseca, and K. Wu, "Broadband substrate integrated waveguide 4×4 Nolen matrix based on coupler delay compensation," *IEEE Trans. Microw. Theory Techn.*, vol. 59, no. 7, pp. 1740–1745, Jul. 2011, doi: 10.1109/TMTT.2011.2142320.

[76] H. Ren, H. Zhang, Y. Jin, Y. Gu, and B. Arigong, "A novel 2-D 3×3 Nolen matrix for 2-D beamforming applications," *IEEE Trans.*

*Microw. Theory Techn.*, vol. 67, no. 11, pp. 4622–4631, Nov. 2019, doi: 10.1109/TMTT.2019.2917211.

[77] J. Hirokawa and N. J. G. Fonseca, "Generalized one-dimensional parallel switching matrices with an arbitrary number of beams," *IEEE J. Microw.*, vol. 1, no. 4, pp. 975–988, Oct. 2021, doi: 10.1109/JMW.2021.3106871.

[78] K. Wu, M. Bozzi, and N. J. G. Fonseca, "Substrate integrated transmission lines: Review and applications," *IEEE J. Microw.*, vol. 1, no. 1, pp. 345–363, Jan. 2021, doi: 10.1109/JMW.2020.3034379.

[79] C. C. Chang, R. H. Lee, and T. Y. Shih, "Design of a beam switching/steering Butler matrix for phased array system," *IEEE Trans. Antennas Propag.*, vol. 58, no. 2, pp. 367–374, Feb. 2010, doi: 10.1109/TAP.2009.2037693.

[80] H. N. Chu and T. Ma, "An extended 4×4 Butler matrix with enhanced beam controllability and widened spatial coverage," *IEEE Trans. Microw. Theory Techn.*, vol. 66, no. 3, pp. 1301–1311, Mar. 2018, doi: 10.1109/TMTT.2017.2772815.

[81] K. Ding and A. A. Kishk, "Extension of Butler matrix number of beams based on reconfigurable couplers," *IEEE Trans. Antennas Propag.*, vol. 67, no. 6, pp. 3789–3796, Jun. 2019, doi: 10.1109/TAP.2019.2902668.

[82] J. R. Wallington, "Analysis, design and performance of a microstrip Butler matrix," in *Proc. 3rd Eur. Microw. Conf.*, Oct. 1973, vol. 1, pp. 1–4, doi: 10.1109/EUMA.1973.331648.

[83] Q. Yang et al., "A low complexity 16×16 Butler matrix design using eight-port hybrids," *IEEE Access*, vol. 7, pp. 177,864–177,873, Dec. 2019, doi: 10.1109/ACCESS.2019.2958739.

[84] X. Wang et al., "28 GHz multi-beam antenna array based on wideband high-dimension 16x16 Butler matrix," in *Proc. 13th Eur. Conf. Antennas Propag. (EuCAP)*, 2019, pp. 1–4.

[85] S. Kutty and D. Sen, "Beamforming for millimeter wave communications: An inclusive survey," *IEEE Commun. Surveys Tuts.*, vol. 18, no. 2, pp. 949–973, Secondquarter 2016, doi: 10.1109/COMST.2015.2504600.

[86] J. Zhang, X. Yu, and K. B. Letaief, "Hybrid beamforming for 5G and beyond millimeter-wave systems: A holistic view," *IEEE Open J. Commun. Soc.*, vol. 1, pp. 77–91, 2020, doi: 10.1109/OJCOMS.2019.2959595.

[87] "17 GHz to 22 GHz, 4-beam and 4-element, Ka-band beamformer," Analog Devices, Wilmington, MA, USA, ADAR3000, 2022. [Online]. Available: https://www.analog.com/en/products/adar3000.html

[88] W. Theunissen, V. Jain, and G. Menon, "Development of a receive phased array antenna for high altitude platform stations using integrated beamformer modules," in *Proc. 2018 IEEE/MTT-S Int. Microw. Symp.*, pp. 779–782, doi: 10.1109/MWSYM.2018.8439255.

[89] D. Sikri and R. M. Jayasuriya, "Multi-beam phased array with full digital beamforming for SATCOM and 5G," *Microw. J.*, vol. 60, no. 4, pp. 64–79, 2019.

[90] C. Zhang, F. Zhang, S. Syed, M. Otto, and A. Bellaouar, "A low noise figure 28GHz LNA in 22nm FDSOI technology," in *Proc. 2019 IEEE Radio Freq. Integr. Circuits Symp. (RFIC)*, pp. 207–210, doi: 10.1109/RFIC.2019.8701831.

[91] Z. Chbili and A. Kerber, "Self-heating impact on TDDB in bulk FinFET devices: Uniform vs non-uniform stress," in *Proc. 2016 IEEE Int. Integr. Rel. Workshop (IIRW)*, pp. 45–48, doi: 10.1109/IIRW.2016.7904898.

[92] "16 channel beamforming transceiver RFIC covers the full 57 to 71 GHz unlicensed band," *Microw. J.*, vol. 64, no. 5, pp. 146–150, May 2021. [Online]. Available: https://www.microwavejournal.com/articles/35968-channel-beamforming-transceiver-rfic-covers-the-full-57-to-71-ghz-unlicensed-band

[93] "TRXBF01: Unrivalled ready-to-use WiGig RFIC for 57 – 71 GHz." Sivers Semiconductors. Accessed: Jun. 2020. [Online]. Available: https://www.sivers-semiconductors.com/wp-content/uploads/2021/10/Product-Brief-TRXBF01_202110.pdf?hsCtaTracking=ffd4d4e8-646f-4e9b-bc49-e926707743b8%7C27c0226b-c72e-4e06-a05a-065a2e70370f

[94] A. S. Y. Poon and M. Taghivand, "Supporting and enabling circuits for antenna arrays in wireless communications," *Proc. IEEE*, vol. 100, no. 7, pp. 2207–2218, Jul. 2012, doi: 10.1109/JPROC.2012.2186949.

[95] C. Fulton, M. Yeary, D. Thompson, J. Lake, and A. Mitchell, "Digital phased arrays: Challenges and opportunities," *Proc. IEEE*, vol. 104, no. 3, pp. 487–503, Mar. 2016, doi: 10.1109/JPROC.2015.2501804.

[96] R. Rotman, M. Tur, and L. Yaron, "True time delay in phased arrays," *Proc. IEEE*, vol. 104, no. 3, pp. 504–518, Mar. 2016, doi: 10.1109/JPROC.2016.2515122.

[97] D. R. Martinez, R. A. Bond, and M. M. Vai, *High Performance Embedded Computing Handbook: A Systems Perspective*. Boca Raton, FL, USA: CRC Press, 2018.

[98] K. Kuhlmann, K. Rezer, and A. F. Jacob, "Far field measurement on Ka-band substrate-integrated waveguide antenna array with polarization multiplexing," in *Proc. 2008 IEEE MTT-S Int. Microw. Symp. Dig.*, pp. 1337–1340, doi: 10.1109/MWSYM.2008.4633024.

[99] A. Stark et al., "SANTANA: Advanced electronically steerable antennas at Ka-band," in *Proc. 3rd Eur. Conf. Antennas Propag.*, 2009, pp. 471–478.

[100] "PRIME – Digital beam former ASIC 20." SatixFy. Accessed: Jan. 20, 2022. [Online]. Available: https://www.satixfy.com/prime/

[101] "EV12DD700 – Dual channel Ka-band capable 12 GSps DAC." Teledyne e2v Semiconductors. Accessed: Jun. 2021. [Online]. Available: https://semiconductors.teledyneimaging.com/en/products/digital-to-analog-converters/ev12dd700/

[102] "Prime 2.0 – Digital beamformer ASIC for flexible satellite payloads." SatixFy. Accessed: Sep. 2021. [Online]. Available: https://www.satixfy.com/

[103] E. A. Alwan, S. B. Venkatakrishnan, A. A. Akhiyat, W. Khalil, and J. L. Volakis, "Code optimization for a code-modulated RF front end," *IEEE Access*, vol. 3, pp. 260–273, Apr. 2015, doi: 10.1109/ACCESS.2015.2419195.

[104] T. Zimmer et al., "SiGe HBTs and BiCMOS technology for present and future millimeter-wave systems," *IEEE J. Microw.*, vol. 1, no. 1, pp. 288–298, Jan. 2021, doi: 10.1109/JMW.2020.3031831.

[105] D. Pepe and D. Zito, "Two mm-wave vector modulator active phase shifters with novel IQ generator in 28 nm FDSOI CMOS," *IEEE J. Solid-State Circuits*, vol. 52, no. 2, pp. 344–356, Feb. 2017, doi: 10.1109/JSSC.2016.2605659.

[106] K. Takagi, C. Y. Ng, H. Sakurai, and K. Matstushita, "GaN MMIC for Ka-band with 18W," in *Proc. 2015 IEEE Compound Semicond. Integr. Circuit Symp. (CSICS)*, pp. 1–4, doi: 10.1109/CSICS.2015.7314504.

[107] C. Y. Ng et al., "A 20-Watt Ka-band GaN high power amplifier MMIC," in *Proc. 2014 9th Eur. Microw. Integr. Circuit Conf.*, pp. 404–407, doi: 10.1109/EuMIC.2014.6997878.

[108] B. Schmukler et al., "A high efficiency, Ka-band, GaN-on-SiC MMIC with low compression," in *Proc. 2019 IEEE BiCMOS Compound Semicond. Integr. Circuits Technol. Symp. (BCICTS)*, pp. 1–4, doi: 10.1109/BCICTS45179.2019.8972749.

[109] N. Estella, E. Camargo, J. Schellenberg, and L. Bui, "High-efficiency, Ka-band GaN power amplifiers," in *Proc. 2019 IEEE MTT-S Int. Microw. Symp. (IMS)*, pp. 568–571, doi: 10.1109/MWSYM.2019.8701005.

[110] P. Colantonio and R. Giofré, "A GaN-on-Si MMIC power amplifier with 10W output power and 35% efficiency for Ka-band satellite downlink," in *Proc. 2020 15th Eur. Microw. Integr. Circuits Conf. (EuMIC)*, pp. 29–32, doi: 10.1109/EuMIC48047.2021.00019.

[111] "Design summit 2022." Qorvo. Accessed: May 2022. [Online]. Available: https://www.qorvo.com/

[112] "OMMIC innovating with III-V'S." OMMIC. Accessed: Jun. 2021. [Online]. Available: https://www.ommic.com/

[113] F. Y. Colomb and A. Platzker, "2 and 4 watt Ka-band GaAs PHEMT power amplifier MMICs," in *Proc. 2003 IEEE MTT-S Int. Microw. Symp. Dig.*, vol. 2, pp. 843–846, doi: 10.1109/MWSYM.2003.1212501.

[114] I. Ju, H. Ji, and I. Yom, "Ku-band GaAs MMIC high power amplifier with high efficiency and broadband," in *Proc. 2015 Conf. Microw. Techn. (COMITE)*, pp. 1–4, doi: 10.1109/COMITE.2015.7120324.

[115] K.-K. Ryu, K.-B. Ahn, and S.-C. Kim, "A 4W GaAs power amplifier MMIC for Ku-band satellite communication applications,"

*J. Semicond. Technol. Sci.*, vol. 15, no. 4, pp. 501–505, Aug. 2015, doi: 10.5573/JSTS.2015.15.4.501.

[116] M. Guidry et al., "Demonstration of 30 GHz OIP3/PDC > 10 dB by mm-wave N-polar deep recess MISHEMTs," in *Proc. 2019 14th Eur. Microw. Integr. Circuits Conf. (EuMIC)*, pp. 64–67, doi: 10.23919/EuMIC.2019.8909579.

[117] F. Wang, T.-W. Li, S. Hu, and H. Wang, "A super-resolution mixed-signal Doherty power amplifier for simultaneous linearity and efficiency enhancement," *IEEE J. Solid-State Circuits*, vol. 54, no. 12, pp. 3421–3436, Dec. 2019, doi: 10.1109/JSSC.2019.2937435.

[118] J. Park, S. Kang, and S. Hong, "Design of a Ka-band cascode power amplifier linearized with cold-FET interstage matching network," *IEEE Trans. Microw. Theory Techn.*, vol. 69, no. 2, pp. 1429–1438, Feb. 2021, doi: 10.1109/TMTT.2020.3040385.

[119] F. Wang and H. Wang, "24.6 an instantaneously broadband ultra-compact highly linear PA with compensated distributed-Balun output network achieving >17.8dBm P1dB and >36.6% PAEP1dB over 24 to 40GHz and continuously supporting 64-/256-QAM 5G NR signals over 24 to 42GHz," in *Proc. 2020 IEEE Int. Solid-State Circuits Conf. (ISSCC)*, pp. 372–374, doi: 10.1109/ISSCC19947.2020.9063157.

[120] B. Park et al., "Highly linear mm-wave CMOS power amplifier," *IEEE Trans. Microw. Theory Techn.*, vol. 64, no. 12, pp. 4535–4544, Dec. 2016, doi: 10.1109/TMTT.2016.2623706.

[121] P. Indirayanti and P. Reynaert, "A 32 GHz 20 dBm-PSAT transformer-based Doherty power amplifier for multi-Gb/s 5G applications in 28 nm bulk CMOS," in *Proc. 2017 IEEE Radio Freq. Integr. Circuits Symp. (RFIC)*, pp. 45–48, doi: 10.1109/RFIC.2017.7969013.

[122] S. N. Ali, P. Agarwal, J. Baylon, S. Gopal, L. Renaud, and D. Heo, "A 28GHz 41%-PAE linear CMOS power amplifier using a transformer-based AM-PM distortion-correction technique for 5G phased arrays," in *Proc. 2018 IEEE Int. Solid-State Circuits Conf. (ISSCC)*, pp. 406–408, doi: 10.1109/ISSCC.2018.8310356.

[123] M. Vigilante and P. Reynaert, "A wideband class-AB power amplifier with 29–57-GHz AM–PM compensation in 0.9-V 28-nm bulk CMOS," *IEEE J. Solid-State Circuits*, vol. 53, no. 5, pp. 1288–1301, May 2018, doi: 10.1109/JSSC.2017.2778275.

[124] S. Shakib, M. Elkholy, J. Dunworth, V. Aparin, and K. Entesari, "2.7 A wideband 28GHz power amplifier supporting 8×100MHz carrier aggregation for 5G in 40nm CMOS," in *Proc. 2017 IEEE Int. Solid-State Circuits Conf. (ISSCC)*, pp. 44–45, doi: 10.1109/ISSCC.2017.7870252.

[125] S. M. A. Ali and S. M. R. Hasan, "A 38-GHz millimeter-wave double-stacked HBT class-F–1 high-gain power amplifier in 130-nm SiGe-BiCMOS," *IEEE Trans. Microw. Theory Techn.*, vol. 68, no. 7, pp. 3039–3044, Jul. 2020, doi: 10.1109/TMTT.2020.2988874.

[126] T.-W. Li, M.-Y. Huang, and H. Wang, "Millimeter-wave continuous-mode power amplifier for 5G MIMO applications," *IEEE Trans. Microw. Theory Techn.*, vol. 67, no. 7, pp. 3088–3098, Jul. 2019, doi: 10.1109/TMTT.2019.2906592.

[127] B. Rabet and J. Buckwalter, "A high-efficiency 28GHz outphasing PA with 23dBm output power using a triaxial balun combiner," in *Proc. 2018 IEEE Int. Solid-State Circuits Conf. (ISSCC)*, pp. 174–176, doi: 10.1109/ISSCC.2018.8310240.

[128] C. R. Chappidi, X. Wu, and K. Sengupta, "Simultaneously broadband and back-off efficient mm-wave PAs: A multi-port network synthesis approach," *IEEE J. Solid-State Circuits*, vol. 53, no. 9, pp. 2543–2559, Sep. 2018, doi: 10.1109/JSSC.2018.2841977.

[129] S. Hu, F. Wang, and H. Wang, "2.1 A 28GHz/37GHz/39GHz multiband linear Doherty power amplifier for 5G massive MIMO applications," in *Proc. 2017 IEEE Int. Solid-State Circuits Conf. (ISSCC)*, pp. 32–33, doi: 10.1109/ISSCC.2017.7870246.

[130] C. Li, O. El-Aassar, A. Kumar, M. Boenke, and G. M. Rebeiz, "LNA design with CMOS SOI process-l.4dB NF K/Ka band LNA," in *Proc. 2018 IEEE/MTT-S Int. Microw. Symp. (IMS)*, pp. 1484–1486, doi: 10.1109/MWSYM.2018.8439132.

[131] Z. Li et al., "A 24–30-GHz TRX front-end with high linearity and load-variation insensitivity for mm-wave 5G in 0.13-µm SiGe BiCMOS," *IEEE Trans. Microw. Theory Techn.*, vol. 69, no. 10, pp. 4561–4575, Oct. 2021, doi: 10.1109/TMTT.2021.3101232.

[132] A. A. Nawaz, J. D. Albrecht, and A. Çağrı Ulusoy, "A Ka/V band-switchable LNA with 2.8/3.4 dB noise figure," *IEEE Microw. Wireless Compon. Lett.*, vol. 29, no. 10, pp. 662–664, Oct. 2019, doi: 10.1109/LMWC.2019.2939540.

[133] F. Inanlou, C. T. Coen, and J. D. Cressler, "A 1.0 V, 10–22 GHz, 4 mW LNA utilizing weakly saturated SiGe HBTs for single-chip, low-power, remote sensing applications," *IEEE Microw. Wireless Compon. Lett.*, vol. 24, no. 12, pp. 890–892, Dec. 2014, doi: 10.1109/LMWC.2014.2361662.

[134] A. Alhamed, O. Kazan, G. Gültepe, and G. M. Rebeiz, "A multiband/multistandard 15-57 GHz receive phased-array module based on 4 x 1 beamformer IC and supporting 5G NR FR2 operation," *IEEE Trans. Microw. Theory Techn.*, vol. 70, no. 3, pp. 1732–1744, Mar. 2022, doi: 10.1109/TMTT.2022.3200415.

[135] T. A. Ozkan, A. Burak, I. Kalyonc, M. Kaynak, and Y. Gurbuz, "A high-gain SiGe BiCMOS LNA for 5G in-band full-duplex applications," in *Proc. 2020 15th Eur. Microw. Integr. Circuits Conf. (EuMIC)*, pp. 53–56.

[136] V. Issakov and A. Werthof, "A 10 mW LNA with temperature compensation for 24 GHz radar applications in SiGe BiCMOS," in *Proc. 2020 IEEE BiCMOS Compound Semicond. Integr. Circuits Technol. Symp. (BCICTS)*, pp. 1–4, doi: 10.1109/BCICTS48439.2020.9392906.

[137] Q. Ma, D. M. W. Leenaerts, and P. G. M. Baltus, "Silicon-based true-time-delay phased-array front-ends at Ka-band," *IEEE Trans. Microw. Theory Techn.*, vol. 63, no. 9, pp. 2942–2952, Sep. 2015, doi: 10.1109/TMTT.2015.2458326.

[138] A. A. Alhamed and G. M. Rebeiz, "A 28–37 GHz triple-stage transformer-coupled SiGe LNA with 2.5 dB minimum NF for low power wideband phased array receivers," in *Proc. 2020 IEEE BiCMOS Compound Semicond. Integr. Circuits Technol. Symp. (BCICTS)*, pp. 1–4, doi: 10.1109/BCICTS48439.2020.9392929.

[139] J. Zhang, D. Zhao, and X. You, "Analysis and design of a CMOS LNA with transformer-based integrated notch filter for *Ku*-band satellite communications," *IEEE Trans. Microw. Theory Techn.*, vol. 70, no. 1, pp. 790–800, Jan. 2022, doi: 10.1109/TMTT.2021.3126858.

[140] H. Chen, H. Zhu, L. Wu, Q. Xue, and W. Che, "A 7.2–27.3 GHz CMOS LNA with 3.51 ±0.21 dB noise figure using multistage noise matching technique," *IEEE Trans. Microw. Theory Techn.*, vol. 70, no. 1, pp. 74–84, Jan. 2022, doi: 10.1109/TMTT.2021.3121074.

[141] J.-F. Chang and Y.-S. Lin, "A 13.7-mW 21-29-GHz CMOS LNA with 21.6-dB gain and 2.74-dB NF for 28-GHz 5G systems," *IEEE Microw. Wireless Compon. Lett.*, vol. 32, no. 2, pp. 137–140, Feb. 2022, doi: 10.1109/LMWC.2021.3121020.

[142] Z. Deng, J. Zhou, H. J. Qian, and X. Luo, "A 22.9–38.2-GHz dual-path noise-canceling LNA with 2.65–4.62-dB NF in 28-nm CMOS," *IEEE J. Solid-State Circuits*, vol. 56, no. 11, pp. 3348–3359, Nov. 2021, doi: 10.1109/JSSC.2021.3102602.

[143] Y. Wang et al., "A Ka-band SATCOM transceiver in 65-nm CMOS with high-linearity TX and dual-channel wide-dynamic-range RX for terrestrial terminal," *IEEE J. Solid-State Circuits*, vol. 57, no. 2, pp. 356–370, Feb. 2022, doi: 10.1109/JSSC.2021.3096190.

[144] H.-W. Choi, C.-Y. Kim, and S. Choi, "6.7–15.3 GHz, high-performance broadband low-noise amplifier with large transistor and two-stage broadband noise matching," *IEEE Microw. Wireless Compon. Lett.*, vol. 31, no. 8, pp. 949–952, Aug. 2021, doi: 10.1109/LMWC.2021.3092742.

[145] H. Chen, H. Zhu, L. Wu, W. Che, and Q. Xue, "A wideband CMOS LNA using transformer-based input matching and pole-tuning technique," *IEEE Trans. Microw. Theory Techn.*, vol. 69, no. 7, pp. 3335–3347, Jul. 2021, doi: 10.1109/TMTT.2021.3074160.

[146] L. Pace et al., "DC power-optimized Ka-band GaN-on-Si low-noise amplifier with 1.5 dB noise figure," *IEEE Microw. Wireless Compon. Lett.*, vol. 32, no. 6, pp. 555–558, Jun. 2022, doi: 10.1109/LMWC.2021.3139769.